ADVANCED OPTICAL MATERIALS
www.advopticalmat.de

Highly Efficient Spintronic Terahertz Emitter Enabled by Metal–Dielectric Photonic Crystal

Zheng Feng, Rui Yu, Yu Zhou, Hai Lu, Wei Tan, Hu Deng, Quancheng Liu, Zhaohui Zhai, Liguo Zhu, Jianwang Cai,* Bingfeng Miao, and Haifeng Ding**

Spintronic terahertz (THz) emitter provides the advantages such as apparently broader spectrum, significantly lower cost, and more flexibility compared with the commercial THz emitters, and thus attracts great interest recently. In past few years, efforts have been made in optimizing the material composition and structure geometry, and the conversion efficiency has been improved close to that of ZnTe crystal. One of the drawbacks of the current designs is the rather limited laser absorption—more than 50% energy is wasted and the conversion efficiency is thus limited. Here, a novel device that fully utilizes the laser intensity and significantly improves the conversion efficiency is theoretically proposed and experimentally demonstrated. The device, which consists of a metal–dielectric photonic crystal structure, utilizes the interference between the multiple scattering waves to simultaneously suppress the reflection and transmission of the laser, and to reshape the laser field distributions. The experimentally detected laser absorption and THz generation show one-to-one correspondence with the theoretical calculations. The strongest THz pulse emission that presents a 1.7 times improvement compared to the currently designed spintronic emitter is achieved. This work opens a new pathway to improve the performance of spintronic THz emitter from the perspective of optics.

Terahertz (THz) radiation plays increasingly important roles in both scientific research and practical applications, such as material science,[1–3] biomedicine,[4–6] wireless communication,[7] security imaging,[6,8,9] etc. In all aspects, it is critical to have a wide band, fully controllable THz source with high power. Despite its high importance, the progresses of high-performance THz devices, especially the emitters,[10,11] are still lacking behind. This is in sharp contrast to the well-developed technologies in its neighboring infrared and microwave bands, leaving a gap so-called "terahertz gap." To date, the development of the THz emitters with high power and high efficiency is still one of the foci in the field of THz research.[12,13]

The femtosecond laser driven THz emitter is an important type of THz emitters that is commonly used.[2,6,11] Previously, its generation was mainly based on the nonspin mechanisms, such as the transient electrical currents in photoconductive antennas,[14–18] the optical rectification from electro-optical crystals,[19–24] the plasma oscillations,[25,26] etc. In 2013, Kampfrath et al. demonstrated a new type THz emitter, called spintronic THz emitter, which is based on the spin related effects in ferromagnetic/nonmagnetic (FM/NM) heterostructures.[27] Compared to the conventional nonspin-based THz emitters, the spintronic THz

Dr. Z. Feng, Dr. W. Tan
Microsystem and Terahertz Research Center
CAEP
Chengdu, Sichuan 610200, P. R. China
E-mail: tanwei@mtrc.ac.cn

R. Yu, Dr. B. F. Miao, Prof. H. F. Ding
National Laboratory of Solid State Microstructures
and Department of Physics
Nanjing University
Nanjing, Jiangsu 210093, P. R. China
E-mail: hfding@nju.edu.cn

Y. Zhou, Prof. J. W. Cai
Beijing National Laboratory for Condensed Matter Physics
Institute of Physics
Chinese Academy of Sciences
Beijing 100190, P. R. China
E-mail: jwcai@iphy.ac.cn

Dr. H. Lu
Engineering Laboratory for Optoelectronic Technology and Advanced Manufacturing
Henan Normal University
Xinxiang, Henan 453007, P. R. China

Dr. H. Deng, Q. C. Liu
School of Information Engineering
Southwest University of Science and Technology
Mianyang, Sichuan 621010, P. R. China

Dr. Z. H. Zhai, Dr. L. G. Zhu
Institute of Fluid Physics
China Academy of Engineering Physics
Mianyang, Sichuan 621900, P. R. China

The ORCID identification number(s) for the author(s) of this article can be found under https://doi.org/10.1002/adom.201800965.

DOI: 10.1002/adom.201800965

emitter possesses the additional advantage of the spin freedom of the electron besides that of the charge freedom, opening a new pathway for broadband (up to 30 THz) and controllable THz wave generation.[27] The reported conversion efficiency of the spintronic THz emitter, however, was about two orders of magnitude lower than that of commercial ZnTe crystal. Since then, efforts have been made to improve the performance.[28–30] In 2016, Seifert et al. significantly enhanced the conversion efficiency by choosing NM layer with large spin Hall angle (such as Pt, W), optimizing the layers' thickness as well as introducing $NM_1/FM/NM_2$ trilayer to fully utilize both the backward- and forward-flowing spin currents. They found that a 5.8 nm thick W/CoFeB/Pt trilayer achieved the conversion efficiency close to that of the commercial 1 mm thick ZnTe crystal and outperform it in terms of the bandwidth, flexibility, scalability, and cost.[28] Yang et al. proposed the cascaded multilayer which can generate transient current in each Fe/Pt bilayer structure, leading to considerable power increase.[29] Wu et al. made a comprehensive study on FM/NM bilayer structures, and showed the capability of fabrication on flexible substrates.[30] These optimizations cover from the perspective of both spintronics and THz pulse generation,[28–30] and furthermore, THz beam focusing has been utilized to obtain higher intensity,[31,32] yet the conversion efficiency remains unchanged. On the other hand, the spintronic emitter also involves the laser pumping and absorption processes, which has not been explored yet. In particular, in previous designs,[28–32] the ultrathin metal films only absorb rather limited laser intensity and more than half of the intensity is wasted. To reach higher conversion efficiency, this drawback must be overcome.

Here, we demonstrate a novel scheme to improve the performance of the spintronic THz emitter in turns of power intensity. It utilizes the metal ($NM_1/FM/NM_2$)–dielectric photonic crystal (PhC) structure, where the multiple scatterings suppress the reflection and transmission of the laser light simultaneously, thus maximizing the laser field strength in the metal layers. Since the dielectric interlayer is almost nondissipative, most of the laser energy absorption occurs in the $NM_1/FM/NM_2$ heterostructure, which improves the conversion efficiency of the spintronic emitter. The idea is first presented theoretically with the transfer-matrix method-based model. We further experimentally fabricate a series of PhC samples with different periods and repeats. The measured laser absorbance and the THz amplitude show one-to-one correspondences with the theoretical calculations. At the optimal conditions, the experimentally obtained conversion efficiency of the PhC structures is about 1.7 times as high as that of the single-repeat spintronic THz emitter, demonstrating the validity of the proposed method. Our work opens a new pathway to improve the performance of the optically pumped spintronic emitter from the perspective of optics.

Spintronic THz emitter relies on two fundamental spintronic effects: the ultrafast laser pulse induced spin polarized current generation and the conversion of the spin current to charge current, namely the inverse spin Hall effect.[33,34] **Figure 1**a shows the schematic processes of a typical spintronic THz emitter with a trilayer heterostructure consisting of $NM_1/FM/NM_2$ thin films: (i) a femtosecond laser pulse impinges on the heterostructure and pumps ultrafast spin currents ($J_{s,1}$ and $J_{s,2}$) from the FM layer into the adjacent NM_1 and NM_2 layers; (ii) due to the inverse spin Hall effect, the ultrafast spin currents are converted into transient charge currents ($J_{c,1}$ and $J_{c,2}$) along the y direction, leading to the THz emission out of the structure. In order to maximize the THz emission, $J_{c,1}$ and $J_{c,2}$ should be parallel to form unidirectional charge current, which requires

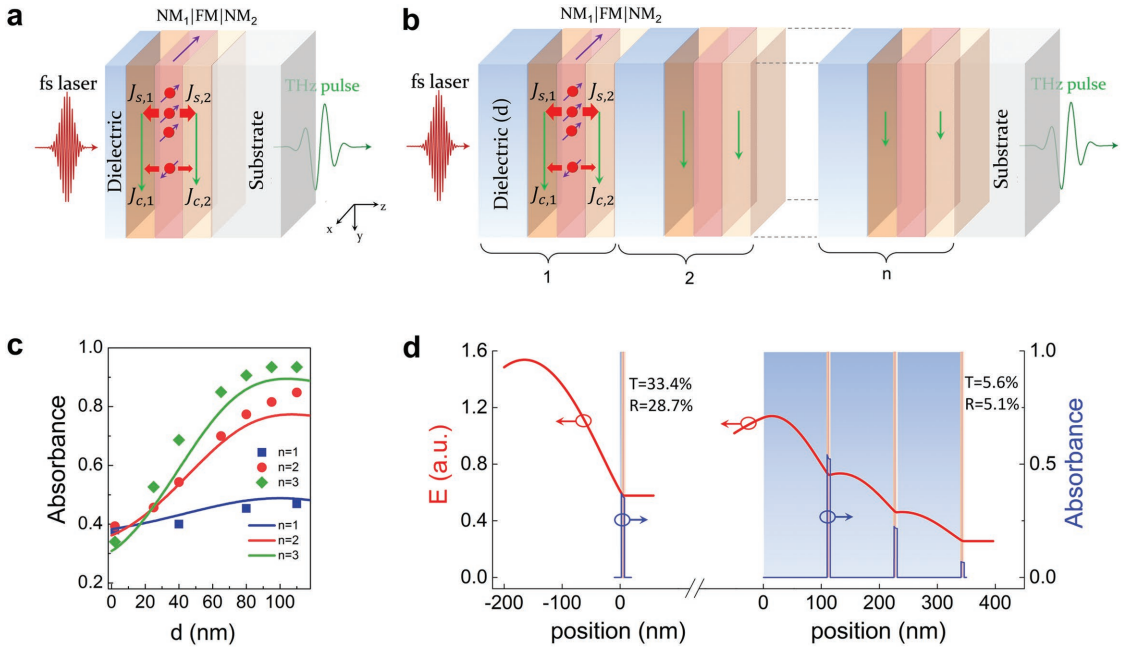

Figure 1. a) Schematic of single-repeat spintronic THz emitter. b) Schematic of the metal–dielectric PhC type spintronic THz emitter. c) The SiO_2 thickness dependent femtosecond laser absorbance for $n = 1, 2, 3$. Symbols are experimental results and solid lines are theoretical calculations. d) The calculated laser field distribution (red) and absorbance in metal layers (blue) of the single-repeat and metal–dielectric PhC type emitter.

the two NM layers to have spin Hall angles with opposite sign. Pt and W have been proved to be a good choice.[28]

In previous works,[28–30] great efforts have been made to maximize the emission efficiency via optimizing the thickness of FM and NM layers. The total thickness of either FM/NM bilayer structure or $NM_1/FM/NM_2$ trilayer structure is suggested to be less than 6 nm.[28–30] This thickness is smaller than the skin depth of the metallic heterostructure and significantly smaller than the laser wavelength (800 nm). As a result, more than half of the incident laser energy is either reflected by or transmitted through the sample, which strongly limits the conversion efficiency. We present a toy model here to offer the evidence. For simplicity, but without losing the generality, we assume that (i) the thickness is negligible compared to the wavelength, and (ii) the dielectric constant of the environment is uniform. According to the boundary conditions and the Maxwell's equations, the reflection and transmission coefficients should satisfy the relation of $1 + r = t$. Consequently, one can deduce that the absorbance, $A = 1 - |r|^2 - |t|^2$, to be ≤50% (see details in Note 1, Supporting Information). Note that this is an intrinsic limitation to the absorbance of ultrathin metal films. To overcome this limit, we propose to use the metal–dielectric PhC structure, where the multiple scatterings and interferences could efficiently suppress the reflection and transmission simultaneously, thus the laser absorption in the metal films is significantly increased.

The schematic of the proposed structure is shown in Figure 1b. It is composed of periodic metal–dielectric films, $[\text{dielectric interlayer}/NM_1/FM/NM_2]_n$, on MgO substrate, where n denotes the number of repeats. In this work, we choose Pt(1.8 nm)/Fe(1.8 nm)/W(1.8 nm) as the THz emitter, which exhibits the largest THz emission efficiency in our experiments, and SiO_2 for the dielectric interlayer. Note that we followed the method established in ref. [28] for optimizing the trilayer THz emitter by varying their individual thicknesses, and the optimized parameters are in good agreement with those in ref. [28] Here we focus on the enhancement based on PhC structure, where the multiple scatterings and interferences can be tailored by adjusting the thickness of the period (d) and the number of repeats (n). Transfer-matrix method is employed for the theoretical calculations and the structure design, which has been proved to be an efficient tool.[28,35]

Since the thickness of each metal film is smaller than its skin depth, the permittivity is most likely different with their bulk values. Thus, we treat the Pt(1.8 nm)/Fe(1.8 nm)/W(1.8 nm) structure as a "single layer" and retrieve its effective permittivity from the measured reflection and transmission coefficients. The model fitting showed that the effective permittivity to be $\varepsilon_m = -29.36 + 24.01i$ (see Note 3, Supporting Information). In the calculation, we also used the bulk value of the permittivity for SiO_2 interlayer and MgO substrate, namely, 2.11 for SiO_2[36] and 2.98 for MgO.[37]

The calculated absorbance, defined as $A = 1 - |r|^2 - |t|^2$, as a function of the thickness of SiO_2 interlayer for a series of samples, n = 1,2,3, is plotted as solid lines in Figure 1c. One can see that for $n = 1$, the absorbance slightly increases with increasing thickness and reaches a maximum at about $d = 100$ nm, yet the maximum absorbance is below 50%. For $n = 2$ and 3, the absorbance increases sharply with increasing thickness of SiO_2 interlayer, and the maximum value increases with the increase in n. It is worth noting that the maximum absorbance for $n = 3$ is almost 90%, about twice of the maximum value for $n = 1$. In contrast, when d is smaller than 25 nm, the absorbance shows inverse relation with n, which decreases with increasing n. This is attributed to the fact that more reflecting interfaces exist and the distance between them does not provide large phase difference to cause significant destructive interference among multireflection waves. Hence, the reflection is considerably enhanced, leading to a reduced absorption.

To gain further insight into the absorption enhancement in the PhC design, we depict in Figure 1d the laser field distribution in two samples: one with $n = 1$ and $d = 2$ nm, which was normally used, and the other one with $n = 3$ and $d = 110$ nm, according to our theoretical design. For the $n = 1$ sample, the reflectance ($R = |r|^2$) and transmittance ($T = |t|^2$) are calculated to be 28.7% and 33.4%, respectively. For the $n = 3$ sample, the laser field distribution is reshaped to suppress the reflection and transmission simultaneously, where $R = 5.1\%$ and $T = 5.6\%$. In comparison with the $n = 1$ sample, the laser field in the first stack of metal films is "lifted," and extended into the second and third stacks, indicating that more incident energies are trapped and absorbed. Therefore, each period can act as an emitter. Since the total thickness of the $n = 3$ sample is less than 350 nm, far smaller than the quarter wavelength of the emitted THz radiation, the induced transient charge currents in each period are in phase, leading to the constructive interference of all emitters. It is expected that the greatly enhanced laser absorption and the superposition of THz emissions would significantly improve the conversion efficiency of the spintronic THz emitter.

A series of samples with n = 1,2,3 and d varying from 2 to 110 nm were fabricated to verify our theoretical proposal. We firstly measured the reflectance and transmittance of the samples under fs laser illumination to obtain their absorbance. The blue squares, red circles, and green diamonds in Figure 1c depicts the fs laser absorbance as a function of SiO_2 thickness d with different repeating periods, n = 1,2,3, respectively. The experimental results exhibit excellent agreement with the theoretical calculations (solid lines). The highest absorbance of the samples with $n = 2$ and $n = 3$ reaches 82% and 93%, respectively. Compared to the typical spintronic emitter, for example, the one with $n = 1$ and $d = 2$ nm, the absorbance in the PhC structures is enhanced by a factor of more than 2.

We then continue with the investigation of the enhancement of THz conversion efficiency. **Figure 2**a–c shows the measured THz pulses generated by the spintronic emitters as a function of SiO_2 thickness d for different repeats, n = 1, 2, 3. To show the effect quantitatively, we define the THz pulse amplitude as the peak to peak intensity and plot its d-dependence for different n in Figure 2d. It is readily to find that the THz pulse amplitude increases with d for each number of period, in accordance with the trend of fs laser absorbance. Nevertheless, the situation becomes quite different if we compare the samples with the same d but different n. For example, when $d = 2$ nm, the THz pulse amplitude of the emitter with $n = 2$ is obviously smaller than that of $n = 1$, whereas they have comparable laser absorbance. When $d > 40$ nm, although the laser absorbance of $n = 2$ is smaller than that of $n = 3$, the emitted THz pulse amplitude is considerably larger. The sample with $n = 2$ and $d = 110$ nm

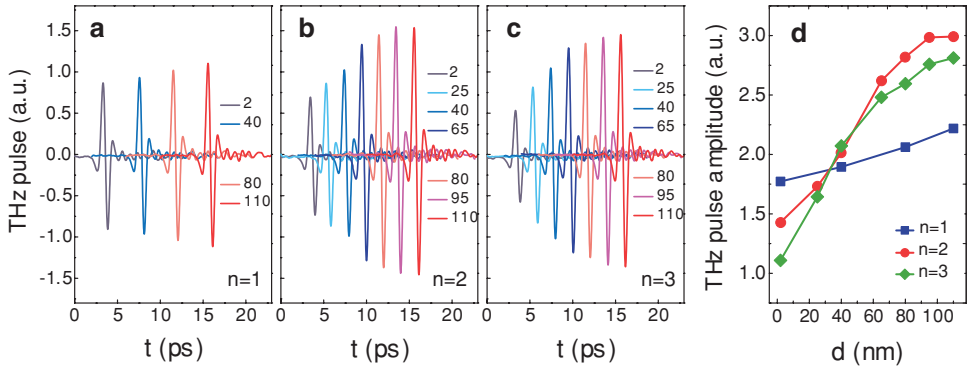

Figure 2. a–c) Experimentally measured *d*-dependent THz pulse generation from samples $[SiO_2(d)/Pt(1.8\ nm)/Fe(1.8\ nm)/W(1.8\ nm)]_n$ with different repeats, namely, $n = 1, 2, 3$. d) *d*-dependent THz pulse amplitude summarized from (a)–(c).

provides the strongest THz pulse emission, which present a 1.7 times improvement compared to the typical single-repeat spintronic THz emitter with $d = 2$ nm.

To make a better comparison, we normalized the THz pulse amplitude and the fs laser absorbance to the values obtained with the single-repeat sample with $d = 2$ nm, which is the typical spintronic THz emitter of current design.[28] Both the experimental (symbols) and theoretically calculated (curves) *d*-dependent normalized quantities are depicted in **Figure 3**a–c. For the samples with $n = 1$, these two normalized values are almost falling into an identical curve, see Figure 3a, which confirms the theoretical proposal that the THz pulse amplitude improvement originates from the fs laser absorbance enhancement. For the samples with $n = 2$ and $n = 3$, although all values increase as increasing *d*, the enhancement rate of the normalized THz pulse amplitude is considerably smaller than that of the normalized fs laser absorbance. And the difference becomes larger as *d* or *n* increases. This phenomenon can be attributed to the absorption and multireflection of the THz radiation by the periodic metal films. In fact, the stack of Pt/Fe/W films not only plays the role of THz emitter, but also reflects and absorbs the THz radiation that passes through it.

In the following, we establish a model to give a quantitative description. Suppose that the THz radiations from the first, second, and third periods are denoted by E_1, E_2, and E_3, respectively, and the corresponding laser absorbance is denoted by A_1, A_2, and A_3, respectively. For the samples with $n = 1$, according to Figure 3a, the emitted THz pulse amplitude is proportional to the laser absorbance. Such linear relation can be expressed as

$$E_{n=1} = E_1 = \beta A_1 \tag{1}$$

where β is a constant, denoting the THz conversion parameter.

For the samples with $n = 2$, multireflection effect should be considered. By measuring the THz transmission and reflection spectra of the structures, we obtained the transmission and reflection coefficients of the stack unit, $t_T = 0.74$, and $r_T = -0.22$, respectively. The THz absorbance can be calculated as $A_T = 1 - |r_T^2| - |t_T^2| = 0.40$. We note that each stack unit will emit THz waves in both forward and backward direction.[28] Hence, the forward THz emission of the whole structure should include three parts: (i) the forward emission from the first stack that experiences multireflection and interference; (ii) the direct forward emission from the second stack; and (iii)

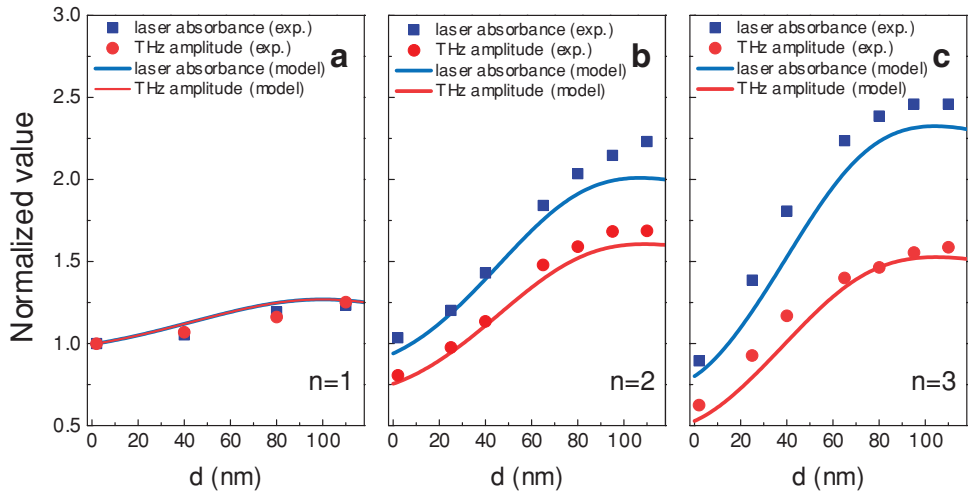

Figure 3. Normalized THz pulse amplitude and femtosecond laser absorbance as the functions of SiO_2 thickness *d* for different repeats: a) $n = 1$, b) $n = 2$, c) $n = 3$. The reference is the sample with $n = 1$ and $d = 2$ nm. Symbols are experimental data and solid lines are the theoretically calculated results.

the backward emission from the second stack that experiences multireflection and interference. The expression can be written analytically (see details in Note 6, Supporting Information)

$$E_{n=2} = \frac{t_T e^{ikd}}{1-r_T^2 e^{2ikd}} E_1 + E_2 + \frac{r_T t_T e^{2ikd}}{1-r_T^2 e^{2ikd}} E_2 \quad (2)$$

where $E_2 = \beta A_2$ and $2kd$ denotes the phase accumulation during one-round reflection. Note that d is far smaller than the THz wavelength. It offers almost zero phase accumulation, leading to constructive interference among multireflections of the emitted wave. Nevertheless, the factor imposed on E_1 as shown in Equation (2) is still smaller than 1 due to absorption and the reflection to the backward direction, resulting in reduction of the contribution of E_1. Meanwhile, as r_T is negative, the third term on the right-hand side of Equation (2), which denotes the contribution of the backward emission from the second period, interferes destructively with the other two forward-emission terms. These two facts are responsible for the reduction of the total THz emission (less than the direct sum of E_1 and E_2). The result is depicted as red solid line in Figure 3b. It explains why the total THz emission is not enhanced linearly with the laser absorbance while increasing n from 1 to 2.

For the PhC structure with $n = 3$, the situation becomes quite complicated. The total forward emission is the sum of the emission from each period and its multireflection contributions. To give the expression more briefly, we employ an approximation here that neglects the multireflections more than two rounds, since $|r_T^5| = 5.2\times10^{-4}$, which is far smaller than 1. Its accuracy was evaluated to be acceptable (see Note 7, Supporting Information). As a result, the expression is approximately given as (see details in Note 7, Supporting Information)

$$\begin{aligned} E_{n=3} = {} & t_T^2 e^{2ikd}\left[\frac{1}{\left(1-r_T^2 e^{2ikd}\right)^2} + \frac{r_T^2 t_T^2 e^{4ikd}}{1-r_T^2 t_T^2 e^{4ikd}} + 4r_T^4 t_T^2 e^{6ikd}\right] \\ & \times \left(E_1 + r_T e^{ikd} E_2 + r_T t_T e^{2ikd} E_3\right) \\ & + t_T e^{ikd}\left(\frac{1}{1-r_T^2 e^{2ikd}} + \frac{r_T^2 t_T^2 e^{4ikd}}{1-r_T^2 t_T^2 e^{4ikd}} + 3r_T^4 t_T^2 e^{6ikd}\right) \\ & \times \left(E_2 + r_T e^{ikd} E_3\right) + E_3 \end{aligned} \quad (3)$$

where $E_3 = \beta A_3$. Note that A_i (i = 1,2,3) can be calculated by employing transfer-matrix method (see Note 5, Supporting Information). The model result is plotted as red solid line in Figure 3c, which shows good agreement with the experimental result. To elucidate the physics more intuitively, we depict the laser field distribution in three samples with $n = 3$ in **Figure 4**, whose SiO_2 thicknesses are 2, 40, and 110 nm, respectively. One can see that: (i) the first period has the largest laser field distribution and thus can provide the strongest THz emission; (ii) with the increase of d, the fields in different periods rise with different rate: A_1 grows most rapidly and A_3 remains almost unchanged. Thus the first period offers the largest THz emission enhancement. Nevertheless, such emission should pass through the other two periods, losing its energy by reflection and absorption. The total contribution is illustrated by the first term on the right-hand side of Equation (3) containing E_1. Furthermore, it is partially cancelled out by the backward emissions from the second and the third period, described by the first term on the right-hand side of Equation (3) containing E_2 and E_3. The second term on the right-hand side of Equation (3) describes the reduction of the contribution of E_2, which shares similar physics with that of E_1. Only the forward emission of E_3, the third term on the right-hand side of Equation (3), contributes to the total emission directly, but it remains almost unchanged with increasing d (see Figure 4). These facts indicate that most laser absorbance enhancement occurs in the first two stacks, but does not make a one-to-one contribution to the total forward THz emission, which is less than the direct sum of E_1, E_2, and E_3. This picture explains why the total THz emission is not enhanced linearly with the laser absorbance while increasing d.

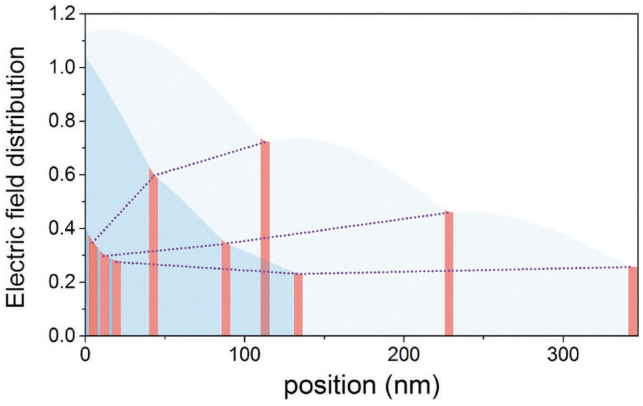

Figure 4. Electric field distributions in the samples [SiO_2(d)/Pt(1.8 nm)/Fe(1.8 nm)/W(1.8 nm)]$_3$ with various SiO_2 thickness, d = 2, 40, 100 nm.

As a result, in our experiments, the sample with $n = 2$ and $d = 110$ nm provides the strongest THz pulse emission, which presents a 1.7 times improvement compared to the typical single-repeat spintronic THz emitter with $n = 1$ and $d = 2$ nm.

In conclusion, we have demonstrated that metal–dielectric PhC structure can greatly enhance the laser absorption in the $NM_1/FM/NM_2$ spintronic THz emitter, and thus improve the conversion efficiency. The key is that the interference between the multiple scattering waves suppresses the reflection and transmission simultaneously and reshapes the laser field distributions in the structure, which can be tailored by tuning the thickness of dielectric interlayer. Accordingly, we achieved the strongest THz pulse emission that presents a 1.7 times improvement compared to the currently designed spintronic THz emitter. A theoretical model was established to elucidate the relationship between the forward THz emission and the laser absorbance for the PhC structures, which showed excellent agreement with experimental results. This work introduces one of the most popular optical concepts, photonic crystal, into the burgeoning research field of spintronic THz emitter, which may inspire the researcher to exploit fruitful ideas in the future, such as plasmonics, metamaterials, etc.

Experimental Section

Sample Preparation: The stack of Pt(1.8 nm)/Fe(1.8 nm)/W(1.8 nm) films and the SiO_2 interlayers were grown on a 0.5 mm thick MgO substrate by dc and rf magnetron sputtering, respectively. The base pressure of the sputter chamber was 5×10^{-5} Pa.

Experimental Details: A standard THz time-domain spectroscopy setup is utilized to generate and detect the THz pulse waveforms. Linearly polarized femtosecond laser pulses (with duration of 120 fs, center wavelength of 800 nm, power of 350 mW, and repetition rate of 80 MHz) from a Ti:sapphire laser oscillator excite the emitter under normal incidence, and the generated THz signals were detected by the electro-optic sampling technique with probe pulses (20 mW) from the same laser copropagating with the THz wave through an electro-optic crystal. A 1 mm thick ZnTe (110) electro-optic crystal was used for detection. An in-plane magnetic field of 140 mT was applied to the emitter. The laser beam diameter was adjusted to be ≈1 mm. For the optical absorption measurements, the emitters were illuminated under the same fs laser energy, and the reflected and transmitted energy were detected by power meter. All measurements were performed at room temperature in a dry air environment.

Supporting Information

Supporting Information is available from the Wiley Online Library or from the author.

Acknowledgements

The authors would like to thank Prof. Jingbo Qi for helpful discussions, and thank Chao Zhou, Min Meng, and Hanbin Wang for experimental assists. This work was supported by Science Challenge Project (Grant No. TZ2018003), the National Natural Science Foundation of China (Grants Nos. 11504345, 11504346, 51571109, 11734006, and 11674379), the National Key R&D Program of China (Grant Nos. 2017YFA0303202 and 2018YFA0306004), and the National Basic Research Program of China (Grant No. 2015CB921403).

Conflict of Interest

The authors declare no conflict of interest.

Keywords

laser absorption, photonic crystals, spintronics, THz emitters, transfer-matrix method

Received: July 24, 2018
Revised: September 8, 2018
Published online: October 9, 2018

[1] B. Ferguson, X. Zhang, *Nat. Mater.* **2002**, *1*, 26.
[2] R. Ulbricht, E. Hendry, J. Shan, T. Heinz, M. Bonn, *Rev. Mod. Phys.* **2011**, *83*, 543.
[3] T. Kampfrath, K. Tanaka, K. Nelson, *Nat. Photonics* **2013**, *7*, 680.
[4] L. Ho, M. Pepper, P. Taday, *Nat. Photonics* **2008**, *2*, 541.
[5] M. Hishida, K. Tanaka, *Phys. Rev. Lett.* **2011**, *106*, 158102.
[6] P. U. Jepsen, D. G. Cooke, M. Koch, *Laser Photonics Rev.* **2011**, *5*, 124.
[7] S. Koenig, D. Lopez-Diaz, J. Antes, F. Boes, R. Henneberger, A. Leuther, A. Tessmann, R. Schmogrow, D. Hillerkuss, R. Palmer, T. Zwick, C. Koos, W. Freude, O. Ambacher, J. Leuthold, I. Kallfass, *Nat. Photonics* **2013**, *7*, 977.
[8] R. Appleby, H. B. Wallace, *IEEE Trans. Antennas Propag.* **2007**, *55*, 2944.
[9] K. B. Cooper, R. J. Dengler, N. Llombart, B. Thomas, G. Chattopadhyay, P. H. Siegel, *IEEE Trans. Terahertz Sci. Technol.* **2011**, *1*, 169.
[10] M. Tonouchi, *Nat. Photonics* **2007**, *1*, 97.
[11] K. Reimann, *Rep. Prog. Phys.* **2007**, *70*, 1597.
[12] X. C. Zhang, A. Shkurinov, Y. Zhang, *Nat. Photonics* **2017**, *11*, 16.
[13] S. S. Dhillon, M. S. Vitiello, E. H. Linfield, A. G. Davies, M. C. Hoffmann, J. Booske, C. paoloni, M. Gensch, P. Weightman, G. P. Willianms, E. Castro-Camus, D. R. S. Cumming, F. Simoens, I. Escorcia-Carranza, J. Grant, S. Lucyszyn, M. Kuwata-Gonokami, K. Konishi, M. Koch, C. A. Schmuttenmaer, T. L. Cocker, R. Huber, A. G. Markelz, Z. D. Taylor, V. P. Wallace, J. A. Zeitler, J. Sibik, T. M. Korter, B. Ellison, S. Rea, P. Goldsmith, K. B. Cooper, R. Appleby, D. Pardo, P. G. Huggard, V. Krozer, H. Shams, M. Fice, C. Renaud, A. Seeds, A. Stöhr, M. Naftaly, N. Ridler, R. Clarke, J. E. Cunningham, M. B. Johnston, *J. Phys. D: Appl. Phys.* **2017**, *50*, 043001.
[14] G. Mourou, C. V. Stancampiano, A. Antonetti, A. Orszag, *Appl. Phys. Lett.* **1981**, *39*, 295.
[15] D. H. Auston, K. P. Cheung, P. R. Smith, *Appl. Phys. Lett.* **1984**, *45*, 284.
[16] Y. C. Shen, P. C. Upadhya, E. H. Linfield, H. E. Beere, A. G. Davies, *Appl. Phys. Lett.* **2003**, *83*, 3117.
[17] A. Dreyhaupt, S. Winnerl, T. Dekorsy, M. Helm, *Appl. Phys. Lett.* **2005**, *86*, 121114.
[18] C. W. Berry, N. Wang, M. R. Hashemi, M. Unlu, M. Jarrahi, *Nat. Commun.* **2013**, *4*, 1622.
[19] X. C. Zhang, Y. Jin, K. Yang, L. J. Schowalter, *Phys. Rev. Lett.* **1992**, *69*, 2303.
[20] A. Rice, Y. Jin, X. F. Ma, X. C. Zhang, D. Bliss, J. Larkin, M. Alexander, *Appl. Phys. Lett.* **1994**, *64*, 1324.
[21] R. A. Kaindl, F. Eickemeyer, M. Woerner, T. Elsaesser, *Appl. Phys. Lett.* **1999**, *75*, 1060.
[22] R. Huber, A. Brodschelm, F. Tauser, A. Leitenstorfer, *Appl. Phys. Lett.* **2000**, *76*, 3191.
[23] T. Tanabe, K. Suto, J. Nishizawa, K. Saito, T. Kimura, *J. Phys. D: Appl. Phys.* **2003**, *36*, 953.
[24] T. Löffler, M. Kreß, M. Thomson, T. Hahn, N. Hasegawa, H. G. Roskos, *Semicond. Sci. Technol.* **2005**, *20*, S134.
[25] X. Xie, J. Dai, X. C. Zhang, *Phys. Rev. Lett.* **2006**, *96*, 075005.
[26] J. Dai, X. Xie, X. C. Zhang, *Phys. Rev. Lett.* **2006**, *97*, 103903.
[27] T. Kampfrath, M. Battiato, P. Maldonado, G. Eilers, J. Nötzold, S. Mährlein, V. Zbarsky, F. Freimuth, Y. Mokrousov, S. Blügel, M. Wolf, I. Radu, P. M. Oppeneer, M. Münzenberg, *Nat. Nanotechnol.* **2013**, *8*, 256.
[28] T. Seifert, S. Jaiswal, U. Martens, J. Hannegan, L. Braun, P. Maldonado, F. Freimuth, A. Kronenberg, J. Henrizi, I. Radu, E. Beaurepaire, Y. Mokrousov, P. M. Oppeneer, M. Jourdan, G. Jakob, D. Turchinovich, L. M. Hayden, M. Wolf, M. Münzenberg, M. Kläui, T. Kampfrath, *Nat. Photonics* **2016**, *10*, 483.
[29] D. Yang, J. Liang, C. Zhou, L. Sun, R. Zheng, S. Luo, Y. Wu, J. Qi, *Adv. Opt. Mater.* **2016**, *4*, 1944.
[30] Y. Wu, M. Elyasi, X. Qiu, M. Chen, Y. Liu, L. Ke, H. Yang, *Adv. Mater.* **2017**, *29*, 1603031.
[31] T. Seifert, S. Jaiswal, M. Sajadi, G. Jakob, S. Winnerl, M. Worf, M. Kläui, T. Kampfrath, *Appl. Phys. Lett.* **2017**, *110*, 252402.
[32] G. Torosyan, S. Keller, L. Scheuer, R. Beigang, E. Th. Papaioannou, *Sci. Rep.* **2018**, *8*, 1311.
[33] J. E. Hirsch, *Phys. Rev. Lett.* **1999**, *83*, 1834.
[34] E. Saitoh, M. Ueda, H. Miyajima, G. Tatara, *Appl. Phys. Lett.* **2006**, *88*, 182509.
[35] C. Zhou, Y. P. Liu, Z. Wang, S. J. Ma, M. W. Jia, R. Q. Wu, L. Zhou, W. Zhang, M. K. Liu, Y. Z. Wu, J. Qi, *Phys. Rev. Lett.* **2018**, *121*, 086801.
[36] C. Z. Tan, *J. Non-Cryst. Solids* **1998**, *223*, 158.
[37] R. E. Stephens, I. H. Malitson, *J. Res. Natl. Bur. Stand.* **1952**, *49*, 249.